journal

J. Am. Ceram. Soc., **85** [10] 2409–16 (2002)

Rheological, Structural, and Stress Evolution of Aqueous Al_2O_3:Latex Tape-Cast Layers

Carlos J. Martinez[†] and Jennifer A. Lewis[*,†,‡]

Materials Science and Engineering Department, Chemical Engineering Department, The Beckman Institute for Advanced Science and Technology, and Frederick Seitz Materials Research Laboratory, University of Illinois, Urbana, Illinois 61801

The rheological, structural, and stress evolution of aqueous alumina (Al_2O_3):latex tape-cast layers of varying composition were studied by shear rheology, direct visualization, and a controlled environment stress measurement device. Their low shear viscosity was nearly independent of the alumina:latex ratio for binary mixtures whose particle size ratio ($\lambda = \bar{D}_{alumina}:\bar{D}_{latex}$) approached unity, but varied over an order of magnitude for systems with particle size asymmetry. Direct visualization of these mixtures revealed that particle flocculation occurred as their total solids loading increased. Their structure was characterized at intermittent points during the drying process by imaging freeze-dried samples using scanning electron microscopy (SEM). Their corresponding stress histories exhibited three distinct regions: an initial period of stress rise, followed by a stress maximum, and, finally, a period of stress decay. Pure alumina layers exhibited a maximum stress of ~1 MPa and a residual stress below 0.01 MPa. Pure latex films exhibited a maximum stress of ~0.1 MPa and only a slight stress decay. The ceramic phase dominated the initial period of stress rise, while the latex phase strongly influenced the residual stress of composite layers cast from alumina:latex suspensions. Their maximum drying stress increased with decreasing Al_2O_3 particle size, whereas their residual stress increased with increasing latex T_g.

I. Introduction

THE tape casting process produces a thin coating on a carrier surface via the doctor blade technique.[1,2] The applied coating dries to form a flexible sheet consisting of a particle-filled, polymeric matrix that may contain appreciable porosity depending on the ceramic-to-binder loading. Tape-cast layers serve as basic building blocks for several laminated ceramic devices including multilayer ceramic packages (MLCs), capacitors (MCCs), structural composites, solid oxide fuel cells, and sensor/actuators.[3]

Aqueous-based tape casting offers several advantages due to the low-cost, nontoxic nature of the fluid vehicle. The development of such formulations has been a subject of recent research.[4–10] Kristoffersen *et al.*[7] evaluated three types of organic binders (i.e., poly(vinyl alcohol), cellulose ethers, and acrylic latex systems) for aqueous tape casting of alumina. They found that latex binders yielded the highest solids loading suspensions, while still maintaining the appropriate rheological behavior. Ushifusa and Cima[11] developed aqueous mullite–acrylic latex suspensions with low organic content for tape casting. Their approach, which emphasized the colloidal nature of the ceramic and organic latex phases in such systems, utilized polyelectrolyte species to improve suspension stability. Most recently, Smay and Lewis[10] developed an aqueous system for tape casting lead zirconate titanate (PZT) layers that also relied on this type of binder system. They investigated the wetting behavior of PZT:latex layers on a mylar carrier surface and their compositional uniformity. Such tapes exhibited a nearly constant PZT:latex ratio through their thickness, despite the large density difference between the PZT and latex particles in suspension.

Aqueous-based tape casting has not been widely adopted by industry, however, because of concerns stemming from drying-related issues (e.g., longer drying times and higher probability of defects such as pinholes and drying cracks relative to nonaqueous systems). Drying is one of the most important steps in the tape casting process. As the liquid vehicle is removed from the green sheet (or layer) via evaporation, the tape undergoes a transformation from its initial fluidlike state to a solidlike, composite layer. To minimize drying-related defects, one must understand how the rheological behavior (which governs the maximum solids loading and, hence, amount of water evaporated during drying), structure, and drying stresses depend on suspension composition.

Aqueous tape casting systems comprising ceramic particles and acrylic latex emulsions can be viewed as binary colloidal suspensions. These complex fluids often display differences in the surface chemistry, colloidal forces, particle morphology, average size and size distribution, and deformability of the individual species. As a simple example, ceramic particles are rigid in nature whereas acrylic latices can undergo deformation in response to shear or capillary stresses.[12–14] To produce suspensions with high solids loading, one must ensure proper stability between ceramic–ceramic, latex–latex, and ceramic–latex particles.[11] Kristoffersson and Carlstrom[6] studied the rheological behavior of four alumina: latex suspensions prepared by blending an alumina powder and acrylic latex binder at two solids volume fractions ($\phi_{ceramic} \sim 0.39$ and 0.48; $\phi_{latex} \sim 0.09$ and 0.13). They found that each suspension exhibited pseudoplastic behavior, where their apparent viscosity and degree of shear thinning increased with increased solids content and binder content. Doreau *et al.*[8] focused on the rheological behavior of Al_2O_3:latex suspensions ($\phi_{total} \sim 0.5$) prepared by mixing an Al_2O_3 powder with blends of acrylic latices of varying glass transition temperature and found that there was little influence of binder content or T_g on suspension rheology. It should be noted that this latter study focused on casting formulations with no variation in mean particle size ratio (λ) between the ceramic and latex phases. In fact, little is known about how the Al_2O_3:latex particle size ratio or the respective volume fractions of these individual constituents would influence suspension rheology and, hence, structure evolution during the casting process.

Rheological measurements have been conducted on bimodal suspensions of granular glass spheres,[15,16] colloidal hard spheres,[17–19] and colloidal soft spheres (rigid particles with long-

V. A. Hackley—contributing editor

Manuscript No. 187321. Received November 16, 2001; approved June 3, 2002.
This research was funded by NSF DMR (#00-71645).
[*]Member, American Ceramic Society.
[†]Materials Science and Engineering Department.
[‡]Chemical Engineering Department, The Beckman Institute for Advanced Science and Technology, and Frederick Seitz Materials Research Laboratory.

range repulsive interactions).[20,21] In all experiments, bimodal suspensions were generated by blending together monodisperse particles of varying size. The key variables that influence their flow are (1) the size ratio (λ) of large-to-small particle diameter, (2) the relative volume fraction of small particles, and (3) their excluded volume (ϕ/ϕ_{max}, where ϕ is the volume fraction of total solids and ϕ_{max} is the maximum solids volume fraction at which flow ceases). For size ratios λ exceeding 10, it is generally accepted that bimodal suspensions exhibit a lower apparent viscosity at a given total solids volume fraction compared with monodisperse suspensions.[20,22] In this case, the smaller particles can easily fit into the interstices formed by the larger particles, and hydrodynamic interactions between different size particles can be neglected. Rodriguez *et al.*[17,18] have shown that even for smaller size ratios (e.g., $\lambda = 2$), the viscosity of bimodal suspensions can be lower than that of monodisperse ones at a given ϕ. Unfortunately, few studies have focused on systems where there are both compositional and particle size differences as well as complexities arising from particle size distributions of each phase. This type of study would bear more relevance for aqueous-based tape casting formulations.

Nahass *et al.*[4] studied the dimensional stability of tape-cast layers deposited from nonaqueous and aqueous alumina suspensions containing the same acrylic binder in soluble form and as a latex emulsion, respectively. Their results suggested that residual stresses developed in the tape-cast layers during drying strongly influence the amount of in-plane dimensional shrinkage that occurs on removal of the tape from the underlying carrier surface. Stress evolution during drying of nonaqueous-based, tape-cast layers has been studied by Lewis and co-workers.[10,23] They found that the binder phase strongly influenced the stress histories of nonaqueous-based, tape-cast layers. Specifically, they showed that the addition of plasticizer species greatly enhanced stress relaxation leading to reductions in both the maximum and residual stresses observed for such layers. Martinez and Lewis[12] have studied shape evolution and stress development in pure latex films of varying T_g and composite (latex-monodisperse silica spheres) films of varying compositions. They observed significant differences in the stress histories of films formed from deformable latices versus rigid silica spheres. They found that composite films exhibited the highest maximum and final stresses at compositions near the critical pigment (filler) volume concentration (CPVC), which occurred at roughly 55% silica by volume. However, the effects of ceramic:latex size ratio coupled with differences in latex T_g on the drying stress behavior of aqueous tape-cast layers has yet to be explored.

Here, the rheological properties, structure, and drying behavior of aqueous-based, Al_2O_3:latex tape-cast layers have been investigated. The influence of suspension composition on the flow behavior of these binary suspensions was characterized through stress viscometry measurements. Next, their structural evolution was examined using a combination of optical microscopy and scanning electron microscopy. Finally, the drying stress behavior of layers of varying composition cast on a rigid support was studied. The measured stress histories were found to be analogous to binder-free, particulate layers during the initial stage of drying.[24,25] However, as drying proceeded, latex coalescence resulted in a transition to behavior characteristic of binder-filled, ceramic films studied previously.

II. Experimental Procedure

(1) Material System

α-Al_2O_3 powders (AKP-15, 30, 50 Sumitomo Chemical Co., NY, NY) with mean particle diameters ($\bar{D}_{alumina}$) of 0.2, 0.4, and 0.7 μm and specific surface areas of 3.8, 7.1, and 10.6 m^2/g, respectively, served as the colloidal phase. Three acrylic latex emulsions (B-1035 and B-1001, Rohm & Haas Co., Philadelphia, PA; and DA-30NA, Dow Chemical Co., Midland, MI) with respective glass transition temperatures of $-40°$, $-6°$, and 19°C, and as-received solids loadings of 55, 55, and 61 vol%, with mean particle diameters ($\bar{D}_{latex}$) of 0.4, 0.33, and 0.2 μm were used in this study. Poly(acrylic acid) (PAA) (Duramax D-3005, Rohm & Haas Co., Philadelphia, PA), with an average molecular weight of 2400 g/mol, was added at a concentration of 0.24 mg of PAA/(m^2 of α-Al_2O_3) to aid ceramic dispersion. Because of the presence of nonadsorbed PAA species in solution, the surface tension was measured to be 58 dyn/cm by the Wilhelmy method.[26]

(2) Suspension Preparation

Pure Al_2O_3 suspensions were prepared by mixing deionized water, PAA, and Al_2O_3 powder, followed by ultrasonication of the suspension at 1 s on/off pulse interval for 300 s. Their pH was adjusted to 9.0 ± 0.1 and they were magnetically stirred for 24 h. Pure latex suspensions were prepared by diluting as-received emulsions with deionized water to a volume fraction of 0.40. The suspension pH was adjusted to 9.0 ± 0.1 by adding appropriate amounts of hydrochloric acid (certified ACS plus, Fisher Scientific, Itasca, IL) or ammonium hydroxide (certified ACS plus, Fisher Scientific, Itasca, IL). Latex suspensions were magnetically stirred for 24 h at room temperature, after which the pH was readjusted if necessary.

Binary suspensions were prepared with different volumetric ratios of Al_2O_3:latex at varying total solids volume fraction (ϕ_{total}). These suspensions were prepared by first mixing deionized water, PAA, and Al_2O_3 in appropriate amounts followed by ultrasonication (Fisher Scientific 550 Sonic Dismembrator, Itasca, IL) at 1-s on/off pulse intervals for 300 s. The suspensions were magnetically stirred for 0.5 h to allow for dispersant adsorption. An appropriate amount of the as-received latex emulsion was then added and the pH adjusted to 9.0 ± 0.1, which yielded the optimal dispersion conditions for both constituents. The resulting suspensions were magnetically stirred for 24 h at room temperature, after which the pH was readjusted as needed.

(3) Rheological Measurements

The rheological behavior of pure Al_2O_3, pure latex, and binary Al_2O_3:latex suspensions was characterized using a controlled stress rheometer (Model Rheolgi CS-50 and CVO, Bohlin, Cranbury, NJ). The measurements utilized either a concentric cylinder (C-25, 0.025–240 Pa) or a double concentric cylinder (double gap, 0.0035–34 Pa) sample geometry at a constant temperature of 22°C. A solvent trap minimized evaporation during each measurement. The rheometer was run in stress viscometry mode and the apparent viscosity (η_{app}) was measured as a function of shear rate in ascending order.

In addition to the results presented, we conducted a series of preliminary experiments to optimize the PAA concentration and solution pH for our system. We found that binary suspensions exhibited the best flow behavior (as characterized by a viscosity minimum and Newtonian flow behavior for $\phi = 0.2$) at a dispersant concentration of 0.24 PAA mg/m^2 of Al_2O_3 and a pH of 9.0 independent of latex volume fraction.

(4) Optical Microscopy

Binary suspensions were diluted to $\phi_{solids} = 0.001$ and observed under an inverted optical microscope (Axiovert 100, Carl Zeiss Inc, Thornwood, NY). A 4 μL drop was placed on a cover slide and imaged using an optical microscope (100× magnification) during drying under ambient conditions (22°C and 36% relative humidity). Images of the microdrop (μ-drop) perimeter were acquired using a digital camera (Color CCD Camera Model XC003, Sony Corp., Japan) and video equipment (Super VHS Model SR-TS1U, JVC Corp., Japan).

(5) Scanning Electron Microscopy of Freeze-Dried Layers

Tape-cast layers (initial thickness = 70 μm) were cast onto a steel substrate (2.54 cm × 2.54 cm × 0.021 cm). They were

then freeze-dried by immersion in liquid nitrogen[27] at intermittent points during the drying process to study their microstructural evolution in the absence of capillary-induced rearrangment. The remaining water was sublimated by placing the freeze-dried samples into a cold vacuum (10^{-3} torr) chamber for 12 h. After sublimation was complete, the samples were warmed to ambient temperature and stored in a low-humidity environment. Their structures were then characterized using scanning electron microscopy (Philips XL30 ESEM-FEG, FEI Corp., Japan).

(6) Stress Measurements

The stress histories of films formed from pure Al_2O_3, pure latex, and Al_2O_3:latex suspensions were measured *in situ* during drying using the cantilever deflection technique, as illustrated in Ref. 12. This device has an environmental chamber that allows for both humidity (15–70 ± 1% relative humidity) and temperature (T = 22°–35° ± 1°C) control. This technique relates the end deflection of a clamped stainless steel substrate to the stress developed in the attached coating as it dries. The end deflection was measured using an optical ensemble consisting of a 1 mW He–Ne laser (Uniphase, Model 1103), a position-sensitive photodiode (UDT Sensors, No. DL-10), an array of mirrors, and a data acquisition computer. Clean, polished steel substrates were mounted onto a movable sample holder fixed at one end. A calibration curve for each substrate was obtained by deflecting the free end of the substrate a known distance using a micrometer. On calibration, the steel substrate was positioned beneath a small doctor blade and the suspension was deposited onto the substrate with a syringe. This assembly was then moved beneath the doctor blade at a constant speed of 1 cm/s to create a coating of the desired initial thickness (300 μm, unless otherwise specified). All films were dried at a 33% relative humidity and a temperature of 25°C.

The biaxial, in-plane (x–y) stress, σ, averaged across the coating thickness is related to the substrate deflection by

$$\sigma = \frac{dEt_s^3}{3t_c l^2(t_s + t_c)(1-\nu)} + \frac{dE_c(t_s + t_c)}{l^2(1-\nu_c)} \tag{1}$$

where d is the end deflection, E is the elastic modulus of the substrate, E_c is the elastic modulus of the coating, t_s is the substrate thickness, t_c is the film height, l is the substrate length, ν is the Poisson ratio of the substrate, and ν_c is the Poisson ratio of the coating. If the modulus of the coating is much smaller than the substrate modulus (as is the case for most particulate films on rigid substrates), this second term can be neglected without introducing a significant error (~1% or less).[28,29] Therefore, only the first term in Eq. (1) was used for our stress data analysis. The stainless steel substrates used had a thickness of 254 μm, and clamped dimensions of 50.8 mm × 6.35 mm with the following properties: E = 1.90 ± 20 GPa, l = 50.8 mm, and ν = 0.36. The reported stress histories have been corrected to account for the contribution of weight loss associated with water evaporation to the measured deflection. Note that the average height of the film (t_c) was used to determine the stress history from the deflection data. The instantaneous film height early in the experiment is greater than the final height; therefore, the stress values are overestimated in the initial stage of the measurement. However, use of this value has little effect on the maximum and residual stress values reported. We have estimated the measurement error for this device to be ~0.010 MPa.[12]

Weight loss measurements were conducted simultaneously on duplicate samples in the cantilever stress chamber during the drying stress measurements. The weight loss data were acquired by suspending the coated substrate from a bottom loading balance (Metler Toledo, Model AG204). The sample mass was recorded every 10 s.

III. Results and Discussion

(1) Rheological Behavior

The apparent viscosity as function of shear rate for pure latex (T_g = −40°C) suspensions of varying latex volume fraction are shown in Fig. 1. These suspensions exhibited behavior characteristic of dispersed systems.[30] At low solids loading ($\phi < 0.3$), Newtonian flow behavior was observed. For $\phi > 0.3$, a transition from Newtonian to shear thinning behavior was observed, where the degree of shear thinning increased with increasing φ. Similar data were obtained for pure suspensions prepared from the three Al_2O_3 powders as well as the other latex systems studied. A plot of relative viscosity ($\dot{\gamma}$ = 1 s^{-1}) as a function of solids volume fraction (ϕ_{solids}) for the latex (T_g = −40°C) and the three Al_2O_3 suspensions is shown in Fig. 2(a). Using the Krieger–Dougherty expression,[31] one can estimate ϕ_{max} for each suspension as follows:

$$\eta_{rel} = \frac{\eta_{app}}{\eta_0} = \left[1 - \frac{\phi}{\phi_{max}}\right]^{-K_H\phi_{max}} \tag{2}$$

where η_{rel} is the relative viscosity, η_{app} is the apparent viscosity of the suspension, η_0 is the apparent viscosity of the solution, φ is the solids volume fraction, ϕ_{max} is the maximum solids volume fraction, and K_H is the hydrodynamic shape factor. We calculated a maximum solids loading ϕ_{max} of ~ 0.6 for pure latex suspensions, and ϕ_{max} values of ~0.56 or less for pure Al_2O_3 suspensions, as reported in Table I, using K_H values of 2.7 and 3.6, respectively. This trend likely reflects differences in the excluded volume occupied by spherical latex particles and the irregularly shaped Al_2O_3 particles with adsorbed PAA. Not surprisingly, one finds that ϕ_{max} for the pure Al_2O_3 suspensions decreased slightly, as their mean particle size decreased. This trend can be understood by considering excluded volume effects stemming from the presence of a steric layer generated by the polyelectrolyte dispersant, whose thickness (δ) is particle size independent.[32] The effective solids volume fraction (ϕ_{eff}) is given by

$$\phi_{eff} = \phi[1 + S\rho_s\delta] \tag{3}$$

where S is the specific surface area of the solid, ρ_s is the solid density, and δ was estimated to be 10 nm.[33,34] Figure 2(b) shows the relative viscosity as a function of ϕ_{eff} for the three Al_2O_3 and the −40°C T_g latex suspensions. These adjusted curves now

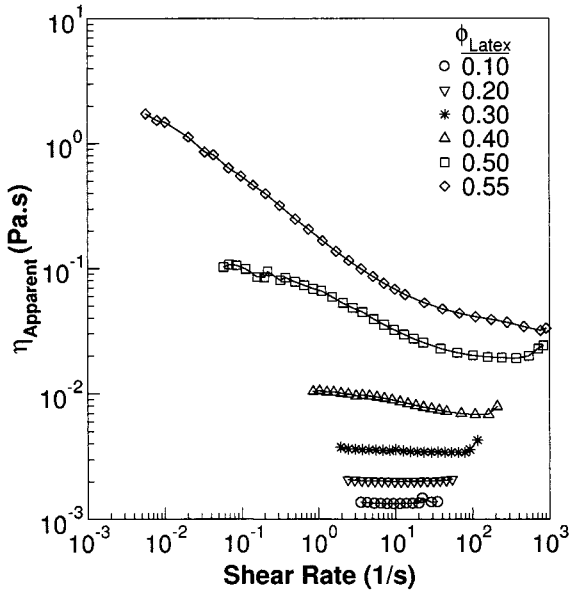

Fig. 1. Log–log plot of apparent viscosity ($\eta_{apparent}$) as a function of shear rate for pure latex (T_g = −40°C) suspensions of varying volume fraction.

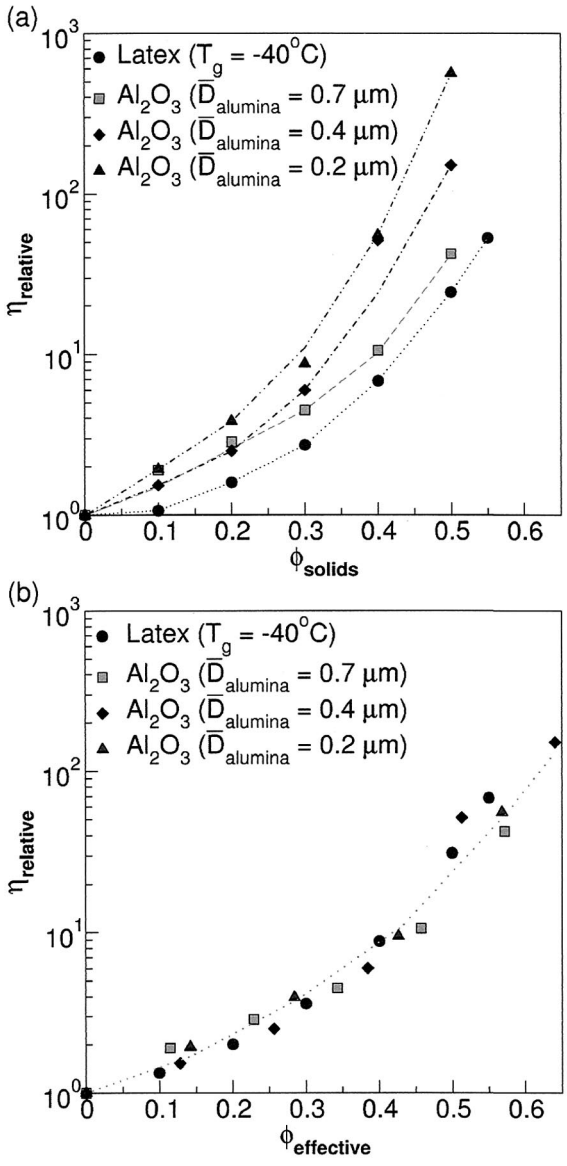

Fig. 2. Relative viscosity ($\eta_{relative}$) as a function of (a) solid volume fraction (ϕ_{solids}) and (b) effective solids volume fraction (ϕ_{eff}), for pure Al_2O_3 suspensions of varying particle size ($\bar{D}_{alumina}$ = 0.2, 0.4, and 0.7 μm) and pure latex suspensions (T_g = −40°C). (Note: Apparent viscosity taken at 1 s^{-1}.)

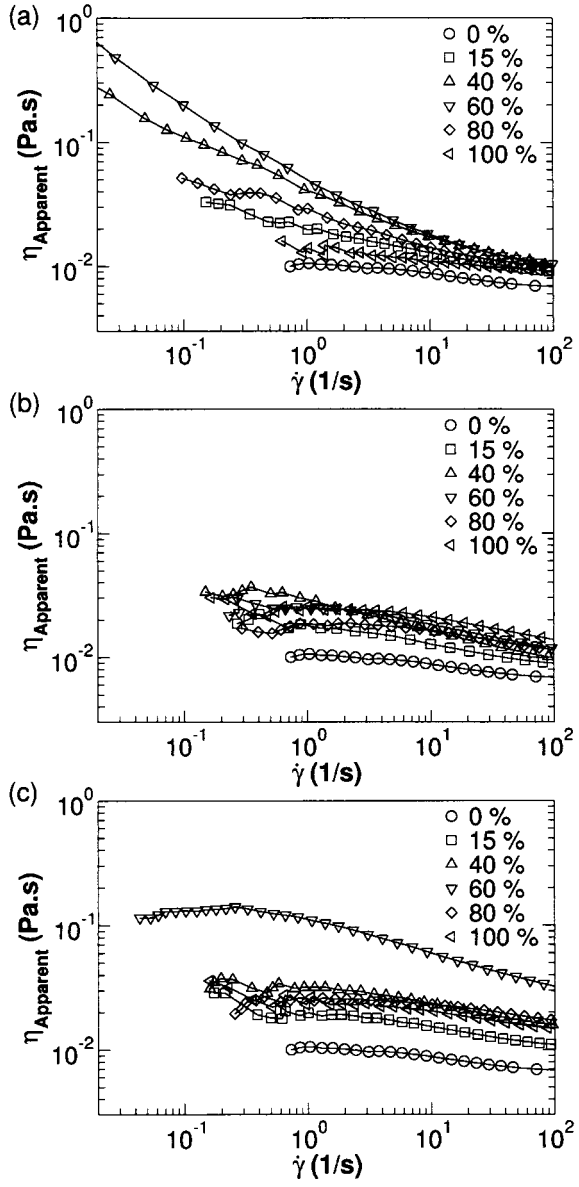

Fig. 3. Log–log plot of apparent viscosity ($\eta_{apparent}$) as a function of shear rate for binary Al_2O_3:latex (ϕ_{total} = 0.4) suspensions with varying composition, (a) AKP-15 ($\bar{D}_{alumina}$ = 0.7 μm):latex ($\bar{D}_{latex}$ = 0.33 μm), (b) AKP-30 ($\bar{D}_{alumina}$ = 0.4 μm):latex ($\bar{D}_{latex}$ = 0.33 μm), and (c) AKP-50 ($\bar{D}_{alumina}$ = 0.2 μm):latex ($\bar{D}_{latex}$ = 0.33 μm). (Note: Suspension composition is specified in terms of % Al_2O_3.)

exhibit universal behavior, with a maximum effective solids (ϕ^{eff}_{max}) ∼ 0.61 observed for all suspensions.

The apparent viscosity of binary suspensions of varying Al_2O_3:latex (T_g = −40°C) ratio and λ with a total solids volume fraction of 0.4 is plotted as a function of shear rate in Fig. 3 for the three Al_2O_3 powders studied. The flow behavior of the Al_2O_3 ($\bar{D}_{alumina}$ = 0.4 μm):latex suspensions (λ = 1) exhibited a nearly Newtonian response with little dependence on the Al_2O_3:latex ratio. In contrast, the Al_2O_3 ($\bar{D}_{alumina}$ = 0.2 μm):latex and Al_2O_3 ($\bar{D}_{alumina}$ = 0.7 μm):latex suspensions (λ ≠ 1) exhibited pseudoplastic behavior. Both their low shear apparent viscosity, which varied over at least 1 order of magnitude, and their degree of shear thinning depended on the Al_2O_3:latex ratio. Interestingly, this behavior was more pronounced for the Al_2O_3 ($\bar{D}_{alumina}$ = 0.7 μm):latex suspensions (λ = 1.75) than the Al_2O_3 ($\bar{D}_{alumina}$ = 0.2 μm):latex suspensions (λ = 0.5). To facilitate direct comparison of these data, we have plotted the apparent suspension viscosity ($\dot{\gamma}$ = 1 s^{-1}) as a function of Al_2O_3 content for each suspension (ϕ_{total} = 0.4) in Fig. 4. The apparent viscosity of the Al_2O_3:latex suspensions decreases slightly relative to that observed for the pure Al_2O_3 suspensions over a narrow compositional range (∼ 60%–90% Al_2O_3). However, on further latex volume percentage increases, the apparent suspension viscosity actually increases beyond that observed for the pure Al_2O_3 suspensions. Their peak viscosity occurred between roughly 40%–60% Al_2O_3. This observation

Table I. Maximum (ϕ_{max}) and Effective Maximum (ϕ^{eff}_{max}) Solids Fraction for Pure Al_2O_3 and Latex Suspensions

Sample	ϕ_{max}	ϕ^{eff}_{max}
Al_2O_3 ($\bar{D}_{alumina}$ = 0.7 μm)	0.56	0.61
Al_2O_3 ($\bar{D}_{alumina}$ = 0.4 μm)	0.53	0.61
Al_2O_3 ($\bar{D}_{alumina}$ = 0.2 μm)	0.50	0.61
Latex (T_g = −40°C)	0.61	0.61
Latex (T_g = −6°C)	0.61	0.61
Latex (T_g = 19°C)	0.61	0.61

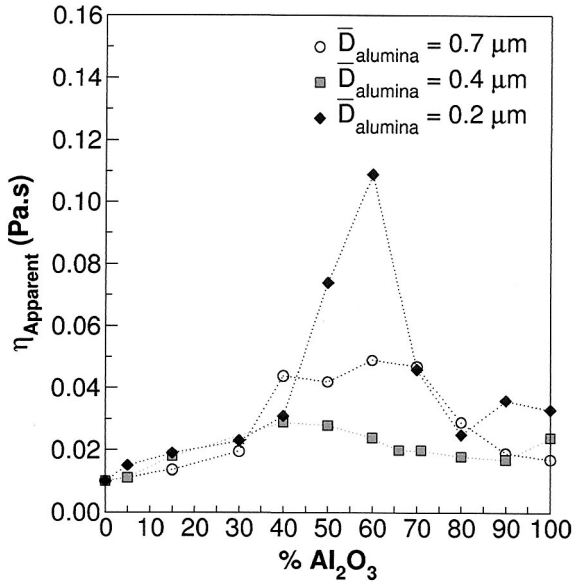

Fig. 4. Apparent viscosity ($\eta_{apparent}$ at a shear rate of 1 s^{-1}) as a function of % Al_2O_3 for binary Al_2O_3:latex (T_g = −40°C) suspensions (ϕ_{total} = 0.4) prepared as a function of varying $\bar{D}_{alumina}$.

sharply contrasts with the behavior observed for blends of monodisperse spheres[15,35] of different size (whose viscosity only decreases on blending). Thus, we believe that our observations likely reflect complications stemming from blending colloids that also have differences in particle size distribution, particle morphology, and surface forces.

(2) Structural Evolution of μ-Droplets

Direct visualization of the structural evolution of highly concentrated suspensions, such as those utilized in tape casting, is difficult because of their highly scattering nature. Therefore, in these experiments, we began our observations using dilute binary suspensions. Using this methodology, we could directly observe the structural evolution of a dilute droplet as it evolves from the supersaturated to saturated state (i.e., as ϕ approaches ϕ_{max}). Figure 5 shows a sequence of images obtained under an inverted optical microscope of the perimeter of a μ-drop deposited from a dilute 2:1 Al_2O_3 ($\bar{D}_{alumina}$ = 0.7 μm):latex (T_g = −40°C) suspension. This image sequence reveals the formation of a dense particle layer (shown in dark brown) that forms at the μ-drop perimeter, as drying proceeds. In related work, Deegan *et al.*[36] have shown that capillary forces wick solvent to this perimeter region to maintain saturation as water evaporation proceeds. As a result, particle migration occurs from the center of the drop to the edge region. The individual particles, represented by small dots in the yellow region, were clearly observed to migrate toward the μ-drop perimeter during the drying process. We found that the width of this dense particle layer increased linearly with time during most of this process (i.e., up to 90% of the total drying time), and increased with an even stronger time dependence beyond that point.

In the latter stage of the drying process, particle clusters were observed to form in the remaining supersaturated region (in yellow) of the μ-drop. These particle clusters were also found to migrate to the drop edge. The pronounced formation of particle clusters indicates that some destabilizing transition has occurred in this (now) more concentrated region in the drop center. Identical behavior was observed for other diluted suspensions prepared from Al_2O_3 powders of varying size and different binary compositions (i.e., 1:1). Similar experiments were also conducted on pure μ-drops deposited from diluted suspensions of the individual constituents only. There was *no* evidence of cluster formation within μ-droplets deposited from pure Al_2O_3 or latex suspensions. The origin of this destabilizing transition therefore appears to be associated with an interaction between the Al_2O_3 and latex particles present in the binary mixtures. It is unclear what drives their flocculation; however, it has important implications on the structure of the tape-cast layers, as described below.

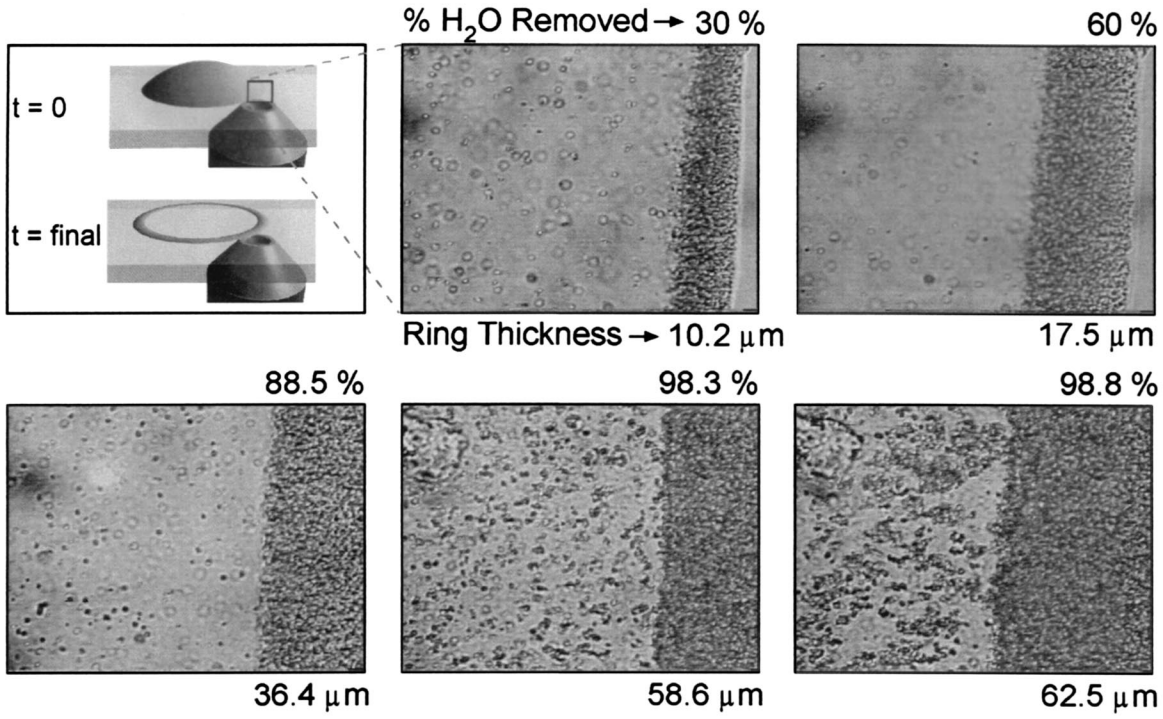

Fig. 5. Optical image sequence of the μ-drop perimeter acquired at different stages of drying. The drop was prepared from a diluted (ϕ_{total} = 0.001) 2:1 Al_2O_3 ($\bar{D}_{alumina}$ = 0.7 μm):latex (T_g = −40°C) suspension. A schematic illustration of the experimental setup, showing an inverted microscope objective focused on the perimeter of the μ-drop at the initial and final stage of drying, is shown on the top left. (Note: The ring thickness and the total amount of H_2O removed are provided for each image.)

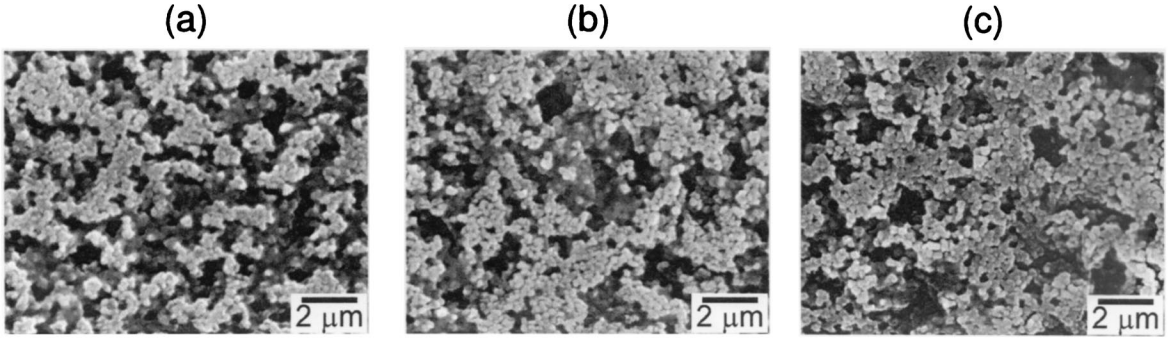

Fig. 6. SEM photomicrographs of the top surface of films cast from 2:1 Al_2O_3 ($\bar{D}_{alumina}$ = 0.4 μm):latex (T_g = −40°C) suspension (ϕ_{total} = 0.4) freeze-dried at intermittent points during drying after (a) 27% water removed by evaporation, (b) 47% removed by evaporation, and (c) 62% removed by evaporation.

(3) Structural Evolution of Tape-Cast Layers

To probe the structural evolution of tape-cast layers at higher concentrations (i.e., those representative of commercial formulations), we obtained images of freeze-dried tape-cast layers using scanning electron microscopy. Figure 6 shows a series of SEM photomicrographs of the top surface of films cast from 2:1 Al_2O_3 ($\bar{D}_{alumina}$ = 0.4 μm):latex (T_g = −40°C) suspensions (ϕ_{total} = 0.4) freeze-dried at intermittent points during the drying process. In all cases, water has been eliminated from the as-cast layers revealing their pore structure. However, the amount of water removed via evaporation versus sublimation varied considerably between these images. Therefore, the extent of capillary driven consolidation experienced by the layers during the drying process also varied. As clearly shown, the top surface of the tape-cast layers appears to be comprised by an assembly of particle clusters, whose interstices provide an open pore structure. The combined structural evidence presented here strongly suggests that that these binary mixtures undergo some type of destabilizing transition at high solids loading. To our knowledge, such observations have not been reportedly previously.

(4) Stress Development in Alumina Layers

The stress history of a representative film prepared from pure Al_2O_3 suspensions ($\bar{D}_{alumina}$ = 0.4 μm, ϕ_{total} = 0.4) is shown in Fig. 7(a). All layers formed exhibited a rapid period of rise in tensile stress (σ_{rise}), followed by a maximum stress (σ_{max}), and subsequent stress decay (σ_{decay}) to a nearly stress-free state. Stress develops during drying because of the constrained volume shrinkage associated with loss of water from the as-cast layer. Because no external loads are applied during this process, mechanical equilibrium requires that the capillary tension developed in the liquid phase exert a compressive force of equal magnitude on the particle network.[37] Since the drying film adheres strongly to the underlying substrate, its contraction occurs only in the *z*-direction, perpendicular to the film plane. The capillary pressure in the liquid is given by Laplace's equation:[38]

$$P_{cap} = 2\gamma/r_p \tag{4}$$

where γ is the liquid/vapor surface tension and r_p is the characteristic pore size. During the period of stress rise, evaporative processes lead to an increased solids volume fraction and corresponding decrease in characteristic pore size within the film. This pore size can be approximated by the hydraulic radius, r_h:[38]

$$r_h = \frac{2(1-\phi)}{\phi\rho_s S} \tag{5}$$

where all parameters have been previously defined. Consolidation persists until the particle network can fully support the drying stress imposed by capillary forces. The stress maximum, σ_{max}, coincides with the time required for the drying film to reach 100% saturation (i.e., $\phi \sim 0.6$), i.e., where further network consolidation essentially ceases. Using Eqs. (4) and (5), one estimates P_{cap} at 100% saturation to be 1.01, 2.03, and 2.9 MPa for the pure Al_2O_3 films with mean particle diameters of 0.7, 0.4, and 0.2 μm, respectively. These values are in reasonable agreement with their respective measured σ_{max} values of 0.4, 1.09, and 1.54 MPa. The period of stress decay following the observed maximum drying stress occurs when liquid menisci retreat into these films, i.e., as their degree of saturation falls below 100%. On the culmination of the drying process, the stress decays to a negligible value.

(5) Stress Development in Latex Films

The stress history of representative films deposited from latex suspensions (ϕ_{total} = 0.4) of varying T_g is shown in Fig. 7. Significant differences in both the magnitude and form of the stress curves were observed between these films and the pure Al_2O_3 films. All latex films exhibited a period of rise in tensile stress (σ_{rise}) that extended throughout most of the weight loss period, i.e., until less than ~10% water remained within the films when a maximum stress (σ_{max}) value was reached. σ_{max} values of 0.074, 0.11, and 0.13 MPa were observed for films with latex T_g's of −40°, −6°, and 19°C, respectively. The onset of σ_{max} occurred during the latter stage of drying, when over 90% of their initial water content had been removed. Little stress decay was seen beyond this point; therefore, their final stress was nearly equivalent to the maximum stress experienced during film formation.

Unlike rigid films, latex films can undergo consolidation well beyond the point where the suspended latex particles first form a touching particle network.[12,13,39] This occurs because the latex particles can deform in response to an applied stress. As stated previously, the tension in the liquid phase must be balanced by the compression of the solid network. A solid network comprised of rigid particles can ultimately support this capillary pressure on reaching its maximum solids loading. In contrast, a solid network comprised of latex particles will deform in response to the tension in the liquid phase provided it is above the minimum film forming temperature (~T_g). Because the solid network deforms, the tension in the liquid phase never reaches the maximum value predicted by Eq. (4). The stress history in this regime depends on the rheological properties of the film and its corresponding strain.[12]

(6) Stress Development in Tape-Cast Layers

The stress history of tape-cast layers deposited from binary suspensions (ϕ_{total} = 0.40) with a 2:1 Al_2O_3:latex ratio and varying Al_2O_3 particle size and latex T_g are shown in Figs. 8(a) and (b), respectively. All layers exhibited a rapid period of rise in tensile stress (σ_{rise}), followed by a maximum stress (σ_{max}), and a subsequent stress decay to a final (residual) stress (σ_{res}). By comparing their stress histories to those obtained for the pure Al_2O_3 and pure latex layers, it is evident that these composite layers include features arising from each of the individual species. For example, their initial stress rise and σ_{max} values depend

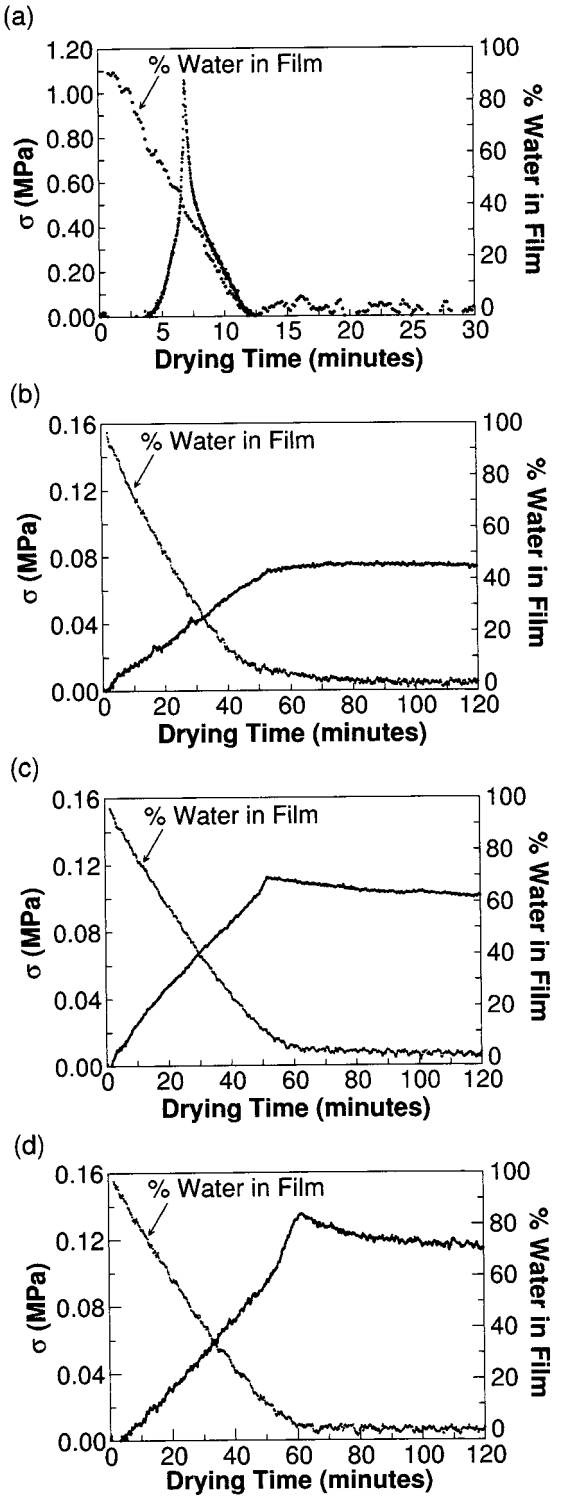

Fig. 7. Stress histories and water content of films prepared from (a) pure Al_2O_3 ($\bar{D}_{alumina}$ = 0.4 μm) suspensions (ϕ_{total} = 0.4) and from pure latex of varying T_g: (b) T_g = −40°C, (c) T_g = −6°C, and (d) T_g = 19°C. (Note: Initial film height = 75 and 300 μm for Al_2O_3 and latex, respectively. Thinner films were required for pure Al_2O_3 to avoid formation of drying cracks.[24])

strongly on the Al_2O_3 mean particle size, as shown in Fig. 9(a). As expected, σ_{max} increases with decreasing particle size. The latex T_g also has a modest influence on σ_{max}, as shown in Fig. 8(b), where σ_{max} increases with increasing T_g. This occurs because the deformation rate of the latex particles is hindered as T_g increases.[13,14] The latex T_g also influences σ_{res} of both pure latex and composite films as shown in Fig. 9(b).

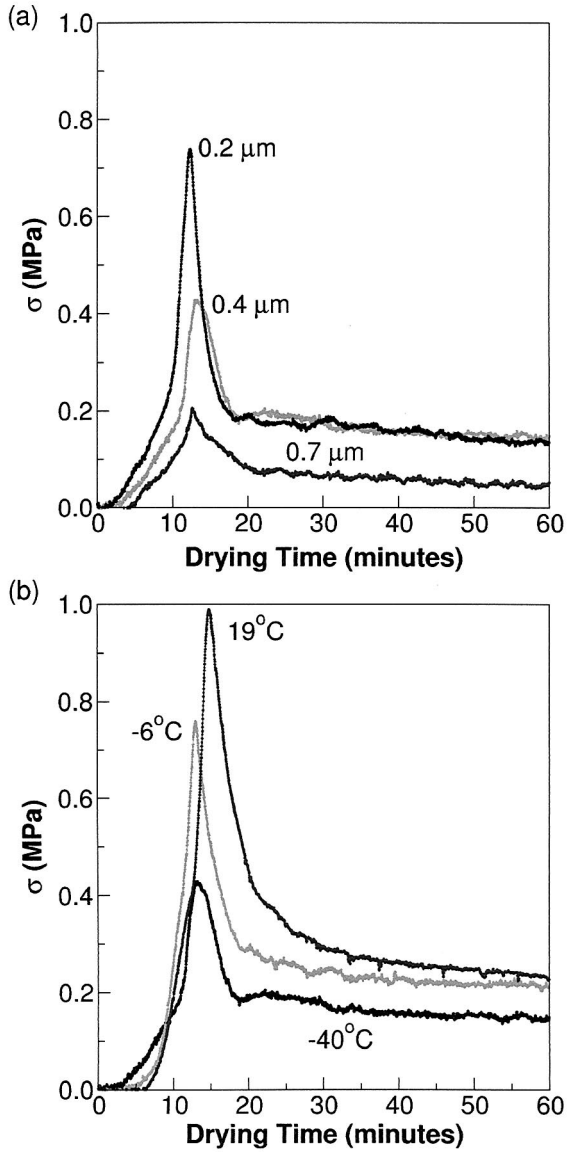

Fig. 8. Stress histories of films prepared from (a) 2:1 Al_2O_3:latex (T_g = −40°C) suspensions (ϕ_{total} = 0.4) with varying Al_2O_3 particle size ($\bar{D}_{alumina}$ = 0.2, 0.4, and 0.7 μm), and (b) 2:1 Al_2O_3 ($\bar{D}_{alumina}$ = 0.4):latex suspensions (ϕ_{total} = 0.4) with varying latex T_g (T_g = −40°, −6°, and 19°C).

IV. Conclusions

We have studied the rheological behavior, structure evolution, and stress development of aqueous-based tape casting layers based on binary mixtures of alumina and latex colloids. Such systems are complex because of variations in surface chemistry, mean particle size and size distribution, particle morphology, and deformability of the individual colloidal species. Such factors influenced their rheological behavior and structural development during film formation. The most striking observation was that these binary mixtures experienced some type of instability as their total solids volume fraction increased. This instability resulted in the formation of particle clusters, which increased suspension viscosity relative to that observed for suspensions comprising the individual constituents. The formation of particle clusters also had a dramatic effect on the green microstructure of the tape-cast layers leading to a more open structure.

The stress histories for pure Al_2O_3, pure latex films, and binary (Al_2O_3:latex) films exhibited a strong compositional dependence. These data offer some insight for improving the dimensional stability of aqueous-based tape-cast layers. We observed the

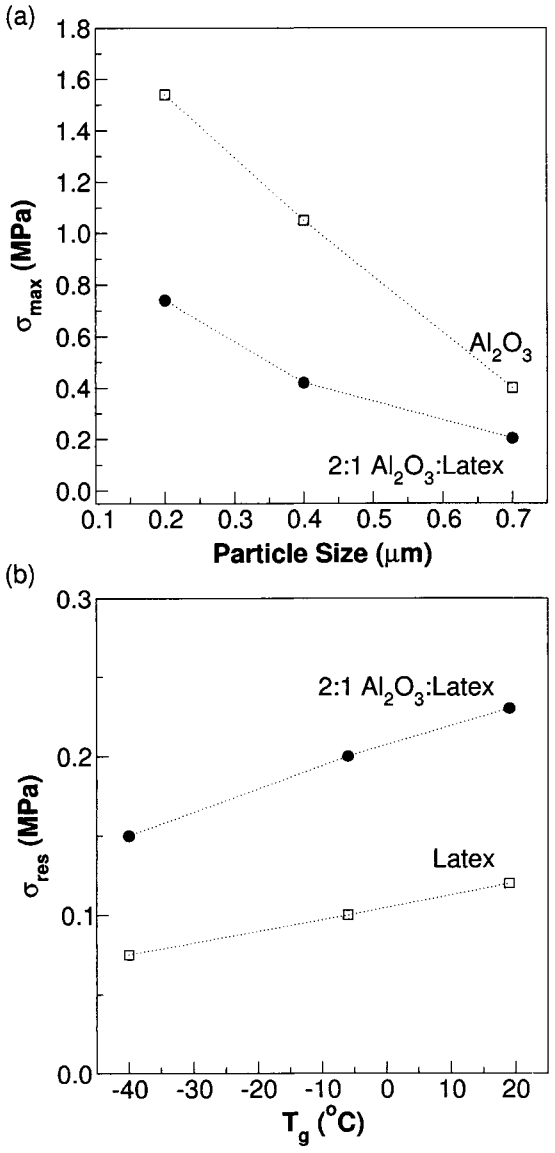

Fig. 9. Plots of (a) maximum stress (σ_{max}) as a function of Al_2O_3 particle size for films prepared from pure Al_2O_3 and 2:1 Al_2O_3 ($\bar{D}_{alumina}$ = 0.2, 0.4, and 0.7 μm):latex (T_g = −40°C) suspensions, and (b) residual stress (σ_{res}) as a function of latex T_g for films prepared from pure latex and 2:1 Al_2O_3 ($\bar{D}_{alumina}$ = 0.4 μm):latex (T_g = −40°, −6°, and 19°C) suspensions.

minimum residual stress for composite layers comprising the largest Al_2O_3 particles and the lowest latex T_g. When dimensional control is critical (e.g., multilayer packaging applications), these material parameters must be carefully tailored. It is recognized, however, that not all applications permit optimization of both parameters. For example, finer particles may be required for emerging components, such as multilayer capacitors with layer thickness on the order of several micrometers. In such systems, dimensional instabilities due to the generation of larger residual stresses must be mitigated solely by tailoring binder properties and drying kinetics.

References

[1]R. E. Mistler, "Tape Casting: The Basic Process for Meeting the Needs of the Electronics Industry," *Am. Ceram. Soc. Bull.*, **69** [6] 1022–26 (1990).

[2]G. N. Howatt, R. G. Breckenridge, and J. M. Brownlow, "Fabrication of Thin Ceramic Sheets for Capacitors," *J. Am. Ceram. Soc.*, **30** [8] 237–42 (1947).

[3]R. E. Mistler, "Tape Casting: Past, Present, Potential," *Am. Ceram. Soc. Bull.*, **77**, 82–86 (1998).

[4]P. Nahass, R. L. Pober, W. E. Rhine, W. L. Robbins, and H. K. Bowen, "Prediction, Explanation of Aging Shrinkage in Tape-Cast Ceramic Green Sheets," *J. Am. Ceram. Soc.*, **75** [9] 2373–78 (1992).

[5]C. Pagnoux, T. Chartier, M. d. F. Granja, F. Doreau, J. M. Ferreira, and J. F. Baumard, "Aqueous Suspensions for Tape-Casting Based on Acrylic Binders," *J. Eur. Ceram. Soc.*, **18**, 241–47 (1998).

[6]A. Kristoffersson and E. Carlstrom, "Tape Casting of Alumina in Water with an Acrylic Latex Binder," *J. Eur. Ceram. Soc.*, **17**, 289–97 (1997).

[7]A. Kristofferson, E. Roncari, and C. Galassi, "Comparison of Different Binders for Water-Based Tape Casting of Alumina," *J. Eur. Ceram. Soc.*, **18,** 2123–31 (1998).

[8]F. Doreau, G. Tari, C. Pagnoux, T. Chartier, and J. M. F. Ferreira, "Processing of Aqueous Tape-Casting of Alumina with Acrylic Emulsion Binders," *J. Eur. Ceram. Soc.*, **18**, 311–21 (1998).

[9]F. Doreau, G. Tari, M. Guedes, T. Chartier, C. Pagnoux, and J. M. F. Ferreira, "Mechanical and Lamination Properties of Alumina Green Tapes Obtained by Aqueous Tape-Casting," *J. Eur. Ceram. Soc.*, **19**, 2867–73 (1999).

[10]J. E. Smay and J. A. Lewis, "Structural and Property Evolution of Aqueous-Based Lead Zirconate Titanate Tape-Cast Layers," *J. Am. Ceram. Soc.*, **84** [11] 2495–500 (2001).

[11]N. Ushifusa and M. Cima, "Aqueous Processing of Mullite-Containing Green Sheets," *J. Am. Ceram. Soc.*, **74** [10] 2443–47 (1991).

[12]C. J. Martinez and J. A. Lewis, "Shape Evolution and Stress Development during Latex–Silica Film Formation," *Langmuir*, in press.

[13]G. L. Brown, "Formation of Films from Polymer Dispersions," *J. Polym. Sci.*, **22**, 423 (1956).

[14]S. T. Eckersley and A. Rudin, "A Mechanism of Film Formation from Polymer Latices," *J. Coat. Technol.*, **61**, 89–100 (1990).

[15]C. Chang and R. L. Powell, "Effect of Particle Size Distributions on the Rheology of Concentrated Bimodal Suspensions," *J. Rheol.*, **38** [1] 85–98 (1994).

[16]A. P. Shapiro and R. F. Probstein, "Random Packing of Spheres and Fluidity Limits of Monodispersed and Bidispersed Suspensions," *Phys. Rev. Lett.*, **68**, 1422–25 (1992).

[17]B. E. Rodriguez and M. S. W. E. W. Kaler, "Binary Mixtures of Monodispersed Latex Dispersions. 2. Viscosity," *Langmuir*, **8**, 2382–89 (1992).

[18]B. E. Rodriguez and E. W. Kaler, "Binary Mixtures of Monodispersed Latex Dispersions. 1. Equilibrium Structure," *Langmuir*, **8**, 2376–81 (1992).

[19]J. Bender and N. J. Wagner, "Reversible Shear Thickening in Monodisperse and Bidisperse Colloidal Dispersions," *J. Rheol.*, **40**, 899–916 (1996).

[20]R. L. Hoffman, "Factors Affecting the Viscosity of Unimodal and Multimodal Colloidal Dispersion," *J. Rheol.*, **36**, 947–65 (1992).

[21]W. J. Hunt and C. F. Zukoski, "The Rheology of Bimodal Mixtures of Colloidal Particles with Long-Range, Soft Repulsions," *J. Colloid Interface Sci.*, **210**, 343–51 (1999).

[22]R. J. Farris, "Prediction of the Viscosity of Multimodal Suspensions from Unimodal Viscosity Data," *Trans. Soc. Rheol.*, **12** [2] 281–301 (1968).

[23]J. A. Lewis, K. A. Blackman, A. L. Ogden, J. A. Payne, and L. F. Francis, "Rheological Property and Stress Development During Drying of Tape-Cast Ceramic Layers," *J. Am. Ceram. Soc.*, **79** [12] 3225–34 (1996).

[24]R. C. Chiu and M. J. Cima, "Drying of Granular Ceramic Films: II, Drying Stress, Saturation Uniformity," *J. Am. Ceram. Soc.*, **76** [11] 2769–77 (1993).

[25]R. C. Chiu, T. J. Garino, and M. J. Cima, "Drying of Granular Ceramic Films: I, Effect of Processing Variables on Cracking Behavior," *J. Am. Ceram. Soc.*, **76** [9] 2257–64 (1993).

[26]N. Pallas and B. Pethica, "The Surface Tension of Water," *Colloids Surf.*, **6** [3] 221–27 (1983).

[27]A. Stanislawska and P. Lepoutre, "Consolidation of Pigmented Coatings: Development of Porous Structure," *Tappi J.*, **79**, 117–25 (1996).

[28]D. Y. Perera and D. V. Eynde, "Considerations on a Cantilever (Beam) Method for Measuring the Internal Stress in Organic Coatings," *J. Coat. Technol.*, **53** [677] 39–44 (1981).

[29]E. M. Corcoran, "Determining Stresses In Organic Coatings Using Plate Beam Deflection," *J. Paint Technol.*, **41** [538] 635–40 (1969).

[30]L. Marshall and C. F. Zukoski, "Experimental Studies on the Rheology of Hard-Sphere Suspensions Near the Glass Transition," *J. Phys. Chem.*, **94**, 1164–71 (1990).

[31]I. M. Krieger and T. J. Dougherty, "A Mechanism for Non-Newtonian Flow in Suspensions of Rigid Spheres," *Trans. Soc. Rheol.*, **3**, 137 (1959).

[32]J. A. Lewis, "Colloidal Processing of Ceramics," *J. Am. Ceram. Soc.*, **83** [10] 2341–59 (2000).

[33]S. Biggs and T. W. Healy, "Electrosteric Stabilization of Colloidal Zirconia with Low-Molecular-Weight Poly(acrylic acid)," *J. Chem. Soc., Faraday Trans.*, **90** [22] 3415–21 (1994).

[34]A. L. Ogden and J. A. Lewis, "Effect of Nonadsorbed Polymer on the Stability of Weakly Flocculated Nonaqueous Suspensions," *Langmuir*, **12** [14] 3413–24 (1996).

[35]J. S. Chong, E. B. Christansen, and A. D. Baer, "Rheology of Concentrated Suspensions," *J. Appl. Polym. Sci.*, **15**, 2007–21 (1971).

[36]R. D. Deegan, O. Bakajin, T. F. Dupont, G. Huber, S. R. Nagel, and T. A. Witten, "Capillary Flow as the Cause of Ring Stains from Dried Liquid Drops," *Nature (London)*, **389** [23] 827–29 (1997).

[37]J. J. Guo and J. A. Lewis, "Aggregation Effects on the Compressive Flow Properties, Drying Behaviour of Colloidal Silica Suspensions," *J. Am. Ceram. Soc.*, **82** [9] 2345–58 (1997).

[38]D. M. Smith, G. W. Scherer, and J. M. Anderson, "Shrinkage during Drying of Silica Gel," *J. Non-Cryst. Solids*, **188**, 191–206 (1995).

[39]D. P. Sheetz, "Formation of Films by Drying of Latex," *J. Appl. Polym. Sci.*, **9**, 3759–73 (1965). □